PROCEEDINGS, 45th Workshop on Geothermal Reservoir Engineering
Stanford University, Stanford, California, February 10-12, 2020
SGP-TR-216

Lessons learned from passive seismic monitoring of EGS Collab Experiment 1

Martin Schoenball[1], Jonathan B. Ajo-Franklin[2], Todd Wood[1], Michelle Robertson[1], Paul Cook[1], Veronica Rodriguez-Tribaldos[1], David Crowe[1], Zhao Hao[1], Timothy Kneafsey[1] and the EGS Collab Team[*]

[1] Lawrence Berkeley National Laboratory, One Cyclotron Rd, Berkeley, CA, 94720, USA
[2] Rice University

schoenball@lbl.gov

Keywords: EGS Collab, Stimulation, Microseismicity

ABSTRACT

Experiment 1 of the EGS Collab project at the Sanford Underground Research Facility was monitored by a 3-D array of sensors deployed in six monitoring and two experimentation boreholes. In total we deployed 25 hydrophones in two borehole strings and one single sensor in the production borehole attached to a SIMFIP probe, 18 3-component accelerometers and about 700 m of fiber optic cables. We recorded data on a total of four digitizers operating in continuous mode: a 96-channel seismograph recording at 4 kHz, a 64-channel digitizer recording at 100 kHz, a 10 kHz digitizer used for the SIMFIP hydrophone and a DAS unit operating at 1 kHz or 10 kHz sampling frequencies. The 100 kHz system has been continuously operating since May 2018 monitoring stimulation periods and long-term flow tests. We achieved an uptime in critical phases of the experiment better than 95% and collected > 700 TB of data which is being processed in near real-time. Here we report on lessons learned from implementing and operating this monitoring system.

1. INTRODUCTION

The U.S. Department of Energy's EGS Collab experiment Enhanced Geothermal System (EGS) Collab project (see Kneafsey et al., 2019 and references therein) aims to improve our understanding of hydraulic stimulations in crystalline rock for enhanced geothermal energy production through execution of intensely-monitored meso-scale experiments. The first experiment is being performed at the 4850 ft level of the Sanford Underground Research Facility (SURF), approximately 1.5 km below the surface in Lead, South Dakota.

For Experiment 1, the objective was to improve our understanding of the formation of hydraulic fractures through an integrated experimental and modelling effort. Experiments included stimulation treatments on the order of minutes to several hours at flow rates of 0.2 to 5 L/min and pressures on the order of 25 MPa. Further, long-term flow tests lasting several months were to be monitored continuously (Kneafsey et al., 2020). The goal of the seismic monitoring was to image fracturing in the host rock through detection and location of picoseismic events and at the same time acquire active seismic and electric data for time-lapse imaging. As such it was designed to image the experimental volume between the injection and production boreholes through a 3-D network of sensors. During the design stages it was unknown how large (or how small) seismic events would be and consequently what their frequency content would be. Preliminary results were described earlier (Schoenball, et al., 2019) and further analyses are presented in Schoenball et al., in prep.

Here we describe our approaches to the seismic monitoring of this experiment and describe successes and learning points for future experiments of this kind, and in particular Experiment 2 of the EGS Collab project.

2. SEISMIC MONITORING SYSTEM

The testbed consists of the production and injection boreholes and six dedicated monitoring boreholes. The borehole trajectories were planned to encompass the experimental volume in 3-D and to cover distances of about 10 m from the injection point. The seismic monitoring array was designed with the goal to deliver sensitive monitoring by small distances between the injection well and the receivers. Furthermore, it was anticipated that seismic events produced during the hydraulic fracturing stimulations would be of very high frequency. The six monitoring boreholes were instrumented with two strings of 12 hydrophones (HTI-96-Min) spaced 1.75 m and 18 3-component piezoelectric accelerometers (PCB 356B18), with three accelerometers deployed in each of the six monitoring

[*] J. Ajo-Franklin, T. Baumgartner, K. Beckers, D. Blankenship, A. Bonneville, L. Boyd, S. Brown, J.A. Burghardt, C. Chai, Y. Chen, B. Chi, K. Condon, P.J. Cook, D. Crandall, P.F. Dobson, T. Doe, C.A. Doughty, D. Elsworth, J. Feldman, Z. Feng, A. Foris, L.P. Frash, Z. Frone, P. Fu, K. Gao, A. Ghassemi, Y. Guglielmi, B. Haimson, A. Hawkins, J. Heise, C. Hopp, M. Horn, R.N. Horne, J. Horner, M. Hu, H. Huang, L. Huang, K.J. Im, M. Ingraham, E. Jafarov, R.S. Jayne, S.E. Johnson, T.C. Johnson, B. Johnston, K. Kim, D.K. King, T. Kneafsey, H. Knox, J. Knox, D. Kumar, M. Lee, K. Li, Z. Li, M. Maceira, P. Mackey, N. Makedonska, E. Mattson, M.W. McClure, J. McLennan, C. Medler, R.J. Mellors, E. Metcalfe, J. Moore, C.E. Morency, J.P. Morris, T. Myers, S. Nakagawa, G. Neupane, G. Newman, A. Nieto, C.M. Oldenburg, T. Paronish, R. Pawar, P. Petrov, B. Pietzyk, R. Podgorney, Y. Polsky, J. Pope, S. Porse, J.C. Primo, C. Reimers, B.Q. Roberts, M. Robertson, W. Roggenthen, J. Rutqvist, D. Rynders, M. Schoenball, P. Schwering, V. Sesetty, C.S. Sherman, A. Singh, M.M. Smith, H. Sone, E.L. Sonnenthal, F.A. Soom, P. Sprinkle, C.E. Strickland, J. Su, D. Templeton, J.N. Thomle, V.R. Tribaldos, C. Ulrich, N. Uzunlar, A. Vachaparampil, C.A. Valladao, W. Vandermeer, G. Vandine, D. Vardiman, V.R. Vermeul, J.L. Wagoner, H.F. Wang, J. Weers, N. Welch, J. White, M.D. White, P. Winterfeld, T. Wood, S. Workman, H. Wu, Y.S. Wu, E.C. Yildirim, Y. Zhang, Y.Q. Zhang, Q. Zhou, M.D. Zoback

boreholes (Figure 1). Additionally, four 3-component geophones (Geospace GS-14L3, 28 Hz resonance frequency) were deployed in sub-vertical boreholes drilled using a jackleg drill. For fiber-optic sensing an eight-strand telecommunication fiber-optic cable with single-mode and mixed-mode fiber strands was deployed. It was interrogated by a Silixa XT-DTS for distributed temperature sensing (DTS), a Silixa iDAS for distributed acoustic sensing (DAS) and an Omnisens DITEST STA-R for distributed strain sensing (DSS).

Other monitoring systems deployed in the monitoring boreholes include 20 automated seismic sources for continuous active source seismic monitoring (CASSM) (Daley et al., 2007), a 3-D electrical resistivity tomography array (Johnson et al., 2019) and thermistors for high precision temperature sensing. The injection and production boreholes were additionally instrumented with 6-component SIMFIP deformation sensors (Guglielmi et al., 2014). The SIMFIP probe in the production borehole also included a single hydrophone interrogated at 10 kHz and an array of electrical conductivity sensors to precisely record the fracture breakthrough location in E1-P.

All sensors and active sources were attached to a 1-inch PVC pipe for conveyance using electrical tape and cable ties (Figure 2). Cables from all deeper sensors would necessarily run past the deployed sensors. The sensors strings were lowered into the HQ sized (96 mm) boreholes and grouted in place.

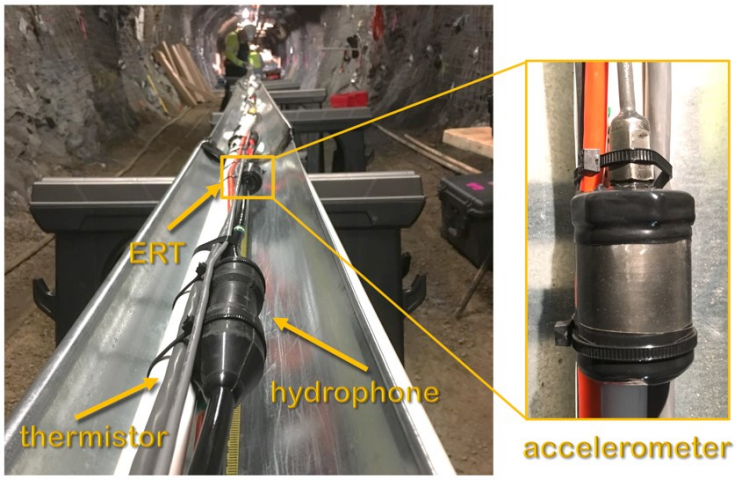

Figure 2: Assembly of monitoring strings with hydrophones and accelerometers fastened to PVC conveyance pipes using cable ties and electrical tape.

The seismic signals were recorded on a total of three digitizers and acquisition systems. The first system is a set of four Geometric Geode seismic recorders for a total of 96 channels and operating at 48 kHz sampling rate. The system operates in triggered mode to record the CASSM surveys and was not used for seismic analysis. A second system (OYO GeoRes) is a conventional 96 channel exploration seismograph and was operating in continuous mode and at 4 kHz sampling rate. The third system is a high-performance 64 channel digitizer (Data Translation VibBox) sampling sensors at 100 kHz with a 24 bit dynamic range. Due to the limited number of recording channels, only 12 of the accelerometers but all of the hydrophones could be connected to the 64-channel 100 kHz recording system. The remaining 4 channels were needed to record control signals of the active sources and the time signal. Further, one hydrophone failed leaving us with 23 operational hydrophones (Figure 1). The 100 kHz system produces a data rate of about 25 MB/s which is stored on 8 TB external hard drives that are replaced every four days.

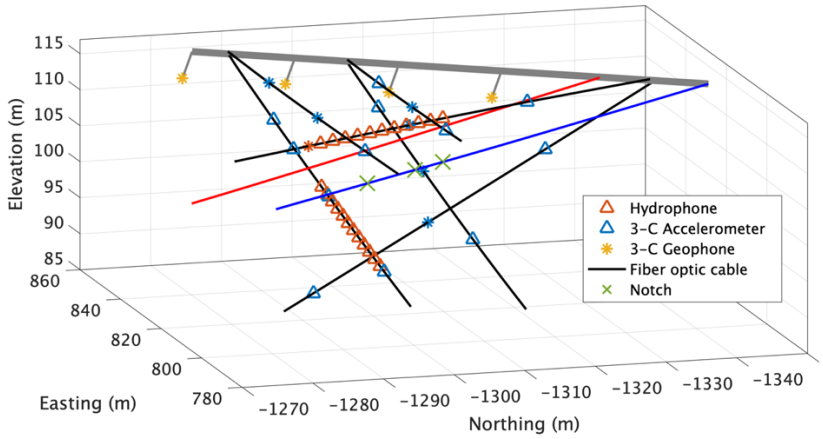

Figure 1: Seismic monitoring setup and notch locations used for stimulation. Stars represent sensors connected only to the 4 kHz system and were not used for subsequent interpretation due to lack of useable signals.

The DAS interrogator was onsite for 2.5 months during April and through June, 2018 when stimulations and flow tests were performed at the location of the 164 ft notch. Data was acquired at sampling rates of 10 kHz or 1 kHz and using 1 m channel spacing. The gauge length, which is basically a moving window over which strain rate is measured, was set to the smallest value possible which was 10 m.

2. PASSIVE SEISMIC OBSERVATIONS

During the injection test dense seismic activity with up to about 10 detected events per second was observed on accelerometer OT16. All other sensors produced far inferior quality data. Hence, only a small fraction of events could be located though owing to the poor signal to noise ratio and consequently the inability to determine phase arrival times. The detected seismic events have their peak energy around 10 kHz, even higher than what was expected during the planning stages (Figure 2).

The geophones did not produce useable signals, even from the stronger active sources. That was not remedied by grouting one of the geophones in its borehole to improve coupling. It is thought that the 5 m deep jackleg-drilled boreholes did not penetrate through the excavation damaged zone of the drift and the rock surrounding the geophones exhibits severe damping. Due to the relatively low sampling rate employed by the 96-channel Geores unit of 4 kHz and the DAS unit (1 or 10 kHz), no useful signals of the active or passive seismic events were recorded by these systems. However, the DAS unit provided useful data of the strain evolution at the very low frequency range ($f \ll 1$ Hz) that will be described elsewhere. Only data the 100 kHz data limited to 64 channels was finally used for seismic analyses.

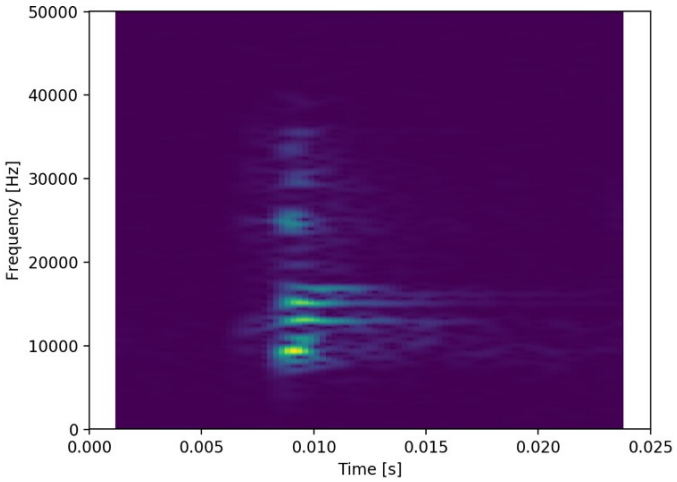

Figure 2: Spectrogram of OB15 trace showing the main energy of the event just below 10 kHz and resonances at higher frequencies approaching the Nyqvist frequency at 50 kHz.

For hydrophones we observe a slight systematic dependence of the number of picks along each sensor string (Figures 3 and 4). Sensor-to-sensor variations of coupling appears to be more important for the usefulness of the recorded signals of the accelerometers. This is especially apparent for accelerometer OT16 which by far outperformed all other sensors in terms of signal-to-noise. As shown in Figure 3 the number of picks obtained from each station does not seem to vary systematically with the distance from the seismic events. For example sensors OT18 and OB15 have vastly different performance, although they are close to each other and at similar distances to the seismicity.

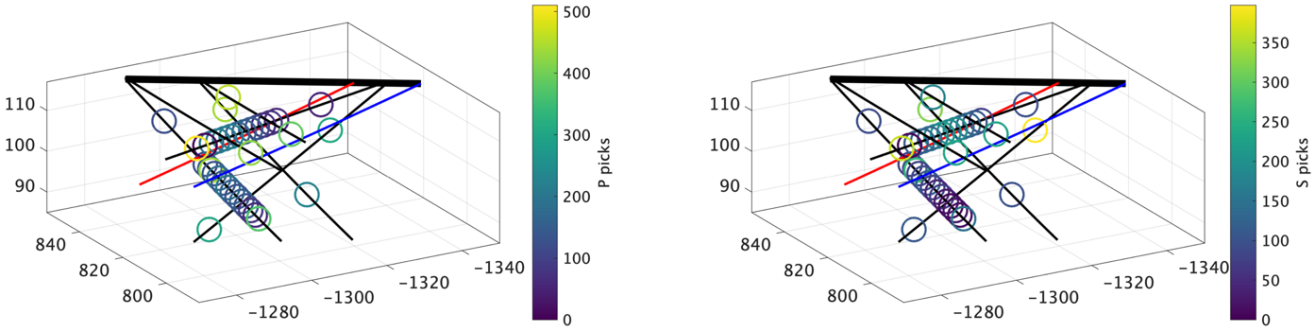

Figure 3: Number of picks by station. While the hydrophones have a systematic relation of the number of picks obtained along each string (highest in the middle of each), we do not observe such a relationship from the accelerometers.

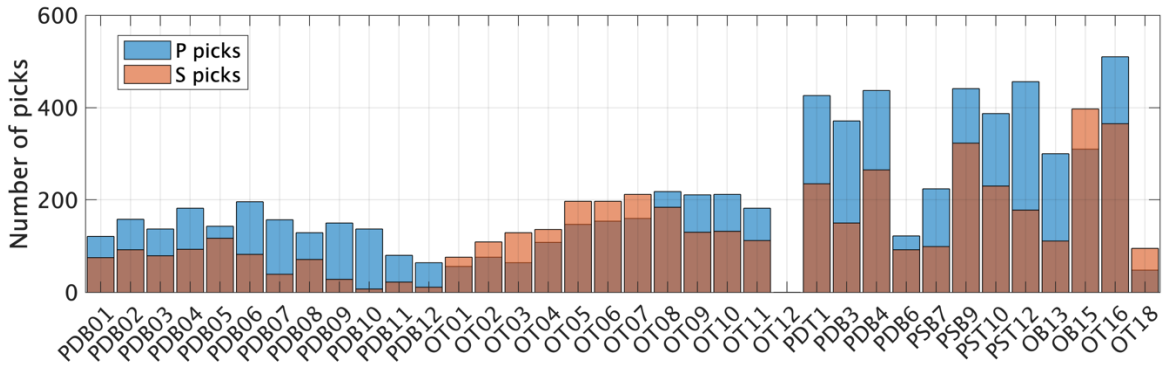

Figure 4: Number of manual picks obtained by each sensor.

One challenging aspect for processing of the seismic data at this site is significant contamination with a variety of coherent noise signals. Besides the active sources, which are easy to remove using their trigger signal, we were also continuously operating the ERT system to obtain time lapse imagery of electrical resistivity before, during, and after the stimulations as well as during long-term flow tests. Since the ERT electrodes are co-located with the sensor cables and are operated with high voltage we observed significant sensor cross-talk. This led to thousands of false triggers per day. Another major source of acoustic noise is drilling activity related to mining operations needed to secure the underground laboratory. A typical jack-leg drill produces about 20 impacts per second, each showing up as individual events in the seismic recordings, and temporarily overloading the processing system with up to 100,000 events per day.

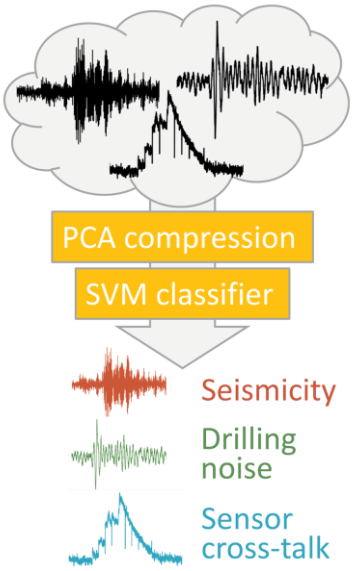

Figure 5: Workflow used for signal discrimination between seismic events and noise signals.

To approach this issue, we have implemented and trained a discriminator based on principal component analysis and a support vector machine (SVM). We assembled a training data set composed of 512 CASSM shots, 1140 drilling impacts, 3214 seismic events, and 5119 ERT cross-talk events. Since the noise signature is different on accelerometers and hydrophones but similar across sensor types we selected three traces of well-performing sensors and discarded the other traces. The selected traces were from hydrophone PDB03 and the X and Z components of accelerometer OT16. This reduced channel set is sufficient to discriminate the signals and it reduces the processing load needed for classification which is particularly important in the real-time application. To extract each signal type's most salient features we used principal component analysis (PCA). PCA works by orthogonally projecting each data point of the waveform onto another 1D subspace, reducing the number of variables needed to convey the most variance within the correlation matrix of a waveform. In our work, we used a block size of 2 and a window size of 1700 samples, each event being represented with 849 components per channel.

To classify the signals, we used a support vector machine approach. The primary mechanism involves identifying a hyper-plane separator which maximizes the distance between support vectors, or data points, closest to the separator. This binary classifier can be extended to multi-class cases by building "one-vs-all" classifiers. A grid search was performed by probing the performance of the SVM model across multiple parameter sets to find the best model (Figure 5).

The final classifier is capable of correctly identifying more than 95 % of ERT and drilling noise. Once trained, the classifier can make its decision in about 0.1 s and is invoked before any picking route is attempted. This reduces the processing load dramatically and

guarantees a short latency between the seismic recording and event localization for real events of interest. The performance of the SVM classifier is promising and we will consider using it during monitoring for Experiment 2.

3. LESSONS LEARNED AND WAY FORWARD

One goal of the passive monitoring was to continuously monitor long-term flow tests. To allow for advanced seismic processing such as ambient noise imaging and others to be applied in the future we strived to collect the entire continuous data set. Rather than only storing triggered events, we collect about 2 TB of continuous data at full sampling rate of 100 kHz. Obviously, this creates challenges of handling these data sets effectively. After initially learning about the difficulties associated with the data set, such as noise, sensor cross-talk and sensor frequency response, we implemented an edge processing workflow which is capable of close to real-time processing. It consists of a lightweight Python stack based on the Obspy package (Krischer et al., 2015) that detects using a standard STA/LTA approach. Using a coincidence trigger that requires at least 20 components to trigger ensures that we are evaluating an event that is strong enough such that an automatic picking algorithm based on the AIC picker would be able to determine P wave arrival times. While the STA/LTA approach is very fast, the picking takes the majority of the overall computational costs. If enough picks are obtained for an event HYPOINVERSE (Klein, 2014) is used to determine its location. An independent 3-D viewer is reading updated catalogs and plots them as soon as new events are detected and located. The entire processing is implemented on a conventional 8 core workstation located in the 4850L drift. In periods of strong activity such as during the December 21, 2018 stimulation, we were accumulating about 20 min of delay between the data recording and localization. For experiment 2 we will optimize the parallelism of this workflow to decrease this delay and allow for a faster response.

After detection, the data is moved to external hard drives. Since these have to be replaced every four days we installed a bank of 10 hard drives to reduce the personnel demand of this task and ensure continuous recordings during longer periods with no personnel underground. Overall, we achieved about 75% availability between May 21, 2018 and August, 2019. This includes scheduled outages earlier in the experiment before effective handling of the instrument cross-talk was implemented (Figure 6). Critical phases of the experiment were covered with about 95% availability. To enable collaboration within the EGS Collab team and the larger community about 700 TB of the data has been uploaded to LBNL's 2 PB RAID server. Collaborators can access this resource using the Globus (www.globus.org) data transfer service. This service enables large data transfers with sustained data rates of 100 MB/s.

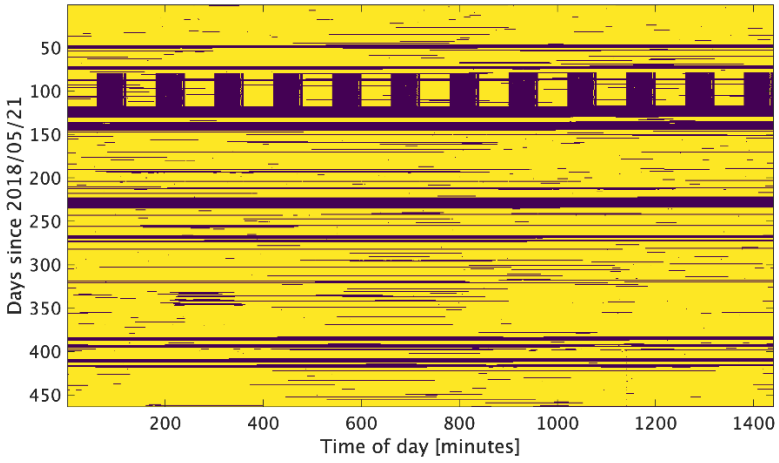

Figure 6: Data availability since the beginning of stimulation experiments on 05/21/2018. Yellow denotes available continuous data and blue denote data gaps.

An important lesson learned was on the frequency content of the passive seismic signals and the sensor response. For the monitoring at meso-scale and appropriate frequencies only a limited range of sensors exist. Seismic sensors sensitive in the 10 kHz range and above include piezoelectric accelerometers and piezoelectric acoustic emission (AE) sensors. Accelerometers work similar to seismometers by having a mass moving against a piezoelectric crystal. The sensor response is determined by the mass of the sensor. There is a trade-off between a linear response to higher frequencies and the sensitivity of the sensor. A higher mass provides a higher sensitivity but leads to lower resonance frequencies, above which no usable signal can be retrieved. The selected accelerometers have a fairly high sensitivity of 1000 mV/g but are specified to be linear only to 5 kHz and with resonance frequencies > 20 kHz. Our own measurements (Figure 7) indicate that the resonance frequency is much lower at about 12 kHz for the Y and Z components and about 8 kHz for the X component. This is precisely where we observe most of the energy of the seismic events. As shown in Figure 2, most seismic energy was detected in the 10 kHz range and energy at higher frequencies results from the resonances of the accelerometers.

For experiment 2 we have to rethink our sensor deployment in order to obtain seismic signals on well-behaved sensors, i.e. sensors that have a linear response in the target frequency range. Considerations are given to accelerometers that are less sensitive but have a linear response function up to higher frequencies. In order to retain or increase the overall sensitivity and record smaller events, these accelerometers would need to be combined with acoustic emission sensors. These sensors derive their signal as the incoming seismic waves deform the piezoelectric crystals which in turn generate a current. Such strategies have been successfully applied to other meso-

scale experiments (Kwiatek et al., 2011, 2018; Villiger et al., 2019). Using this combination of sensors, meaningful magnitudes and even focal mechanisms would be possible to compute events down to the M-4 range.

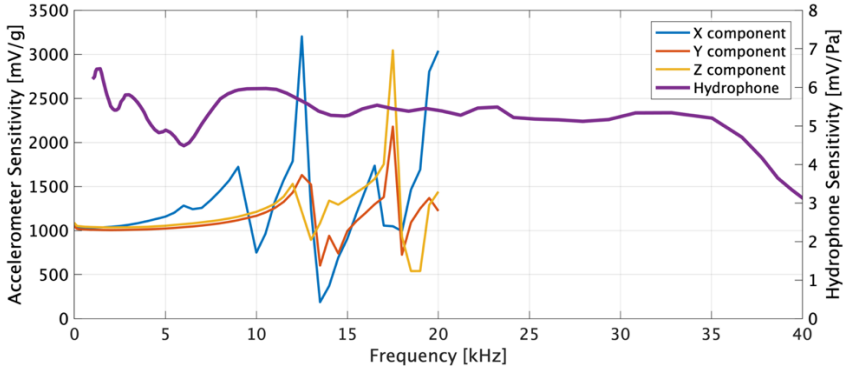

Figure 7: Frequency response curves of accelerometers and hydrophones deployed for Experiment 1.

The CASSM system was continuously operated for most of the experiment and including parts of the long-term flow tests. Each CASSM shot occupies about 0.01 s and travel times to the sensors are less than 0.05 s. With about one CASSM shot per second, we incur only about 5% of downtime, during which the ability to record passive seismic signals would be impacted.

The cross-talk between the ERT system and the seismic acquisition provided for many challenges that are still not fully overcome. In order to be able to run both systems simultaneously in Experiment 2 we will record the ERT system's current pulses on the same digitizer as the accelerometers. Similar to the trigger for the active seismic sources, this signature should allow for an effective method to discard periods where the ERT system was active. Since each pulse only lasts for about 0.01 s, we would incur only minimal downtime and would still be able to monitor the passive wavefield with about 94% coverage which includes downtimes during CASSM activity.

For Experiment 2 it will be important to implement effective means to prevent overload of the real-time processing from drilling impacts. This is particularly crucial since we are expecting a strong increase in mining activity associated with the excavations for the Long-Baseline Neutrino Facility. On the 4850L, not far from the site of Experiment 1, large caverns are going to be excavated beginning in 2020 to install large neutrino detectors.

Other limitations are on the software side. The accuracy of traditional automatic picking algorithms for low signal-to-noise data is often poor. This calls for manual review and refinement of phase picks. However, there is a fast-paced development of a new generation of picking algorithms based on deep learning methods. These have been applied with success by Chai et al. (2020) to the data of Experiment 1. After retraining the PhaseNet convolutional neural network (Zhu & Beroza, 2018) using the manually picked phase arrivals, the algorithm reaches human precision and surpasses the number of picks obtained by manual processing. Implementation of similar methods in real-time processing would be one of the next steps towards better and faster seismic monitoring.

4. CONCLUSIONS

Passive seismic monitoring of Experiment 1 of the EGS Collab project has created a rich dataset accompanied by several challenges. The combination of passive and active geophysical methods and the noise from nearby work as well as mining activities contaminate the passive data and provide numerous challenges for the analysis. However, modern tools such as the Obspy package, parallel computation, and application of machine learning methods, we are able to process these data in near real-time. Planned improvements for Experiment 2 include further implementation of machine learning methods to discard unwanted signals and improved picking algorithms. On the hardware side we will more tightly integrate the multiphysics sensors into the seismic monitoring and consider options to record higher frequencies with greater fidelity.

ACKNOWLEDGEMENTS

This material was based upon work supported by the U.S. Department of Energy, Office of Energy Efficiency and Renewable Energy (EERE), Office of Technology Development, Geothermal Technologies Office, under Award Number DE-AC02-05CH11231 with LBNL. The United States Government retains, and the publisher, by accepting the article for publication, acknowledges that the United States Government retains a non-exclusive, paid-up, irrevocable, world-wide license to publish or reproduce the published form of this manuscript, or allow others to do so, for United States Government purposes. The research supporting this work took place in whole or in part at the Sanford Underground Research Facility in Lead, South Dakota. The assistance of the Sanford Underground Research Facility and its personnel in providing physical access and general logistical and technical support is acknowledged.

REFERENCES

Chai, C., Maceira, M., Santos-Villalobos, H., Venkatakrishnan, S. V., Schoenball, M., & EGS Collab Team. (2020). Automatic Seismic Phase Picking Using Deep Learning for the EGS Collab project. In *45th Workshop on Geothermal Reservoir Engineering,*

Stanford, California.

Daley, T. M., Solbau, R. D., Ajo-Franklin, J. B., & Benson, S. M. (2007). Continuous active-source seismic monitoring of CO2 injection in a brine aquifer. *GEOPHYSICS*, *72*(5), A57–A61. https://doi.org/10.1190/1.2754716

Guglielmi, Y., Cappa, F., Lançon, H., Janowcsyk, J. B., Rutqvist, J., Tsang, C.-F., & Wang, J. S. Y. (2014). ISRM Suggested Method for Step-Rate Injection Method for Fracture In-Situ Properties (SIMFIP): Using a 3-Components Borehole Deformation Sensor. *Rock Mechanics and Rock Engineering*, *47*(1), 303–311. https://doi.org/10.1007/s00603-013-0517-1

Johnson, T. C., Strickland, C., Vermeul, V., Mattson, E., Knox, H. A., Ajo-Franklin, J., et al. (2019). EGS Collab Project Electrical Resistivity Tomography Characterization and Monitoring. In *Proceedings 44th Workshop on Geothermal Reservoir Engineering, Stanford University*.

Klein, F. W. (2014). *User's Guide to HYPOINVERSE-2000, a Fortran Program to Solve for Earthquake Locations and Magnitude* (U. S. Geological Survey, Open File Report 02-171, revised June 2014).

Kneafsey, T. J., Blankenship, D., Knox, H. A., Johnson, T. C., Ajo-Franklin, J., Schwering, P. C., et al. (2019). EGS Collab Project: Status and Progress. In *Proceedings 44th Workshop on Geothermal Reservoir Engineering, Stanford University*.

Kneafsey, T. J., Blankenship, D., Dobson, P. F., Morris, J. P., White, M. D., Fu, P., et al. (2020). The EGS Collab Project: Learning from Experiment 1. In *45th Workshop on Geothermal Reservoir Engineering, Stanford, California*.

Krischer, L., Megies, T., Barsch, R., Beyreuther, M., Lecocq, T., Caudron, C., & Wassermann, J. (2015). ObsPy: a bridge for seismology into the scientific Python ecosystem. *Computational Science & Discovery*, *8*(1), 014003. https://doi.org/10.1088/1749-4699/8/1/014003

Kwiatek, G., Plenkers, K., & Dresen, G. (2011). Source Parameters of Picoseismicity Recorded at Mponeng Deep Gold Mine , South Africa : Implications for Scaling Relations. *Bulletin of the Seismological Society of America*, *101*(6), 2592–2608. https://doi.org/10.1785/0120110094

Kwiatek, G., Martínez-Garzón, P., Plenkers, K., Leonhardt, M., Zang, A., von Specht, S., et al. (2018). Insights Into Complex Subdecimeter Fracturing Processes Occurring During a Water Injection Experiment at Depth in Äspö Hard Rock Laboratory, Sweden. *Journal of Geophysical Research: Solid Earth*, *123*, 6616–6635. https://doi.org/10.1029/2017JB014715

Schoenball, M., Ajo-Franklin, J. B., Robertson, M., Wood, T., Blankenship, D., Cook, P., et al. (2019). *EGS Collab Experiment 1: Microseismic Monitoring*. https://doi.org/10.15121/1557417

Schoenball, M., Ajo-Franklin, J. B., Blankenship, D., Cook, P., Dobson, P. F., Guglielmi, Y., et al. (2019). Microseismic monitoring of meso-scale stimulations for the DOE EGS Collab project at the Sanford Underground Research Facility. In *Proceedings 44th Workshop on Geothermal Reservoir Engineering, Stanford University*.

Schoenball, M., Ajo-Franklin, J., Blankenship, D., Chai, C., Kneafsey, T., Knox, H., Maceira, M., Robertson, M., Sprinkle, P., Strickland, C., Templeton, D., Schwering, P., Ulrich, C., Wood, T., EGS Collab Team (in prep.). Creation of a mixed-mode fracture network at meso-scale through hydraulic fracturing and shear stimulation

Villiger, L., Gischig, V. S., Doetsch, J., Krietsch, H., Dutler, N. O., Jalali, M. R., et al. (2019). Influence of reservoir geology on seismic response during decameter scale hydraulic stimulations in crystalline rock. *Solid Earth*. https://doi.org/10.5194/se-2019-159

Zhu, W., & Beroza, G. C. (2018). PhaseNet: A Deep-Neural-Network-Based Seismic Arrival Time Picking Method. *Geophysical Journal International*. 216, 261-273, https://doi.org/10.1093/gji/ggy423